Microstructure and mechanical properties of laser welded DP600 steel joints

N. Farabi [a], D.L. Chen [a,*], J. Li [b], Y. Zhou [b], S.J. Dong [c]

[a] Department of Mechanical and Industrial Engineering, Ryerson University, 350 Victoria Street, Toronto, Ontario M5B 2K3, Canada
[b] Department of Mechanical and Mechatronics Engineering, University of Waterloo, 200 University Avenue West, Waterloo, Ontario N2L 3G1, Canada
[c] School of Mechanical Engineering, Hubei University of Technology, Wuhan, Hubei, China

ARTICLE INFO

ABSTRACT

To reduce fuel consumption and greenhouse gas emissions, dual phase (DP) steels have been considered for automotive applications due to their higher tensile strength, better initial work hardening along with larger elongation compared to conventional grade of steels. In such applications welding and joining have to be involved, which would lead to a localized alteration of materials and create potential safety and reliability issues under cyclic loading. The aim of this investigation was to evaluate microstructural change after laser welding and its effect on the tensile and fatigue properties in DP600 steel. The welding resulted in a significant increase of hardness in the fusion zone, but also the formation of a soft zone in the outer heat-affected zone (HAZ). While the ductility decreased after welding, the yield strength increased and the ultimate tensile strength remained almost unchanged. Fatigue life at higher stress amplitudes was almost the same between the base metal and welded joints despite slightly lower fatigue limit after welding. Tensile fracture and fatigue failure at higher stress amplitudes occurred at the outer HAZ. Fatigue crack initiation was observed to occur from the specimen surface and crack propagation was characterized by the characteristic mechanism of striation formation. Dimples and deformation bands were observed in the fast propagation area.

© 2009 Elsevier B.V. All rights reserved.

1. Introduction

Increasing concern of environmental safety and reduction of fuel consumption motivate car manufacturers to use lightweight materials having a higher tensile strength coupled with better ductility. By reducing the weight of a car less fuel consumption along with less CO_2 emission can be achieved. Considering the safety standards required in the automobile industry, dual phase (DP) steel has gained its popularity as this steel has a higher tensile strength in conjunction with higher elongation compared to the steel grades of similar yield strength [1]. The microstructure of DP steel consists of soft and ductile ferrite matrix, which is strengthened by hard martensitic phase and possibly bainitic phase with an addition of very little amount of retained austenite [2–6]. The ductility of the steel arises from ferrite and the martensite accounts for the strength.[1] Compared with high strength low alloy (HSLA) steels, DP steel shows slightly lower yield strength but the continuous flow behavior in dual phase steel results in larger and more uniform total elongation, and higher initial work hardening rate along with considerably higher ultimate tensile strength [7]. All these satisfactory mechanical characteristics have made DP steel intriguing to the automobile manufacturers.

It is often stated that more than 50% of a country's gross domestic product is related to welding in one way or another [8] and in the case of the automobile body structure welding is the mostly used joining operation. In previous auto body designs, the most typical material used was mild steel. These car bodies were assembled via resistance spot welding (RSW), a method which fulfilled the demand of automobile manufacturers for high process speed and high volume scenario. But due to the changed material scenario, other welding methods are also gaining popularity in the industry. Due to ease of automation and flexibility laser welding has already gained its reputation in the metal joining field. A significant amount of work has been conducted on the mechanical property of the welded DP steel joined by other welding processes, such as resistance spot welding (RSW) [9–11], laser spot welding [12], gas metal arc welding (GMAW) [13], and friction stir welding [14]. A lot of work can also be found on the laser weldability of DP steel coupled with the effect of welding on the tensile properties [15,16]. But very limited studies on the fatigue properties of these kinds of joints have been reported. In the structural applications the laser welded joints would be prone to failure under cyclic loading conditions, so that the characterization of fatigue resistance of the welded joints is necessary.

---

* Corresponding author. Tel.: +1 416 979 5000x6487; fax: +1 416 979 5265.
E-mail address: dchen@ryerson.ca (D.L. Chen).
[1] The microstructural matrix of DP steel is developed after annealing in the so-called intercritical temperature range where ferrite and austenite are established. This process is then followed by rapid cooling to transform from austenite to martensite [2,4].

Table 1
Chemical composition (in wt%) of the DP600 steel selected in the present study.

C	Mn	Si	Al	Mo	Cr	Cu	S
0.09	1.84	0.36	0.05	0.01	0.02	0.03	0.005

Previous studies on DP steels showed that the welding led to the formation of soft zone in the sub-critical area of the heat-affected zone (HAZ), and the mechanical properties of the welded joints were significantly affected by this area [17,18]. The tensile properties and formability of the welded joints were seriously hindered by the formation of this softened zone [17–20]. The tensile tests carried out in this study also corroborated such findings. Then the questions arose on whether the soft zone would lead to a reduction in the fatigue resistance and to what extent. Detailed studies concerning the fatigue properties and the effect of soft zone on the failure behavior of the welded DP joints are lacking. For the effective applications of DP steels, a comprehensive study of their fracture characteristics and mechanisms under both monotonic and cyclic loads is of vital importance. Therefore, the present study was aimed at evaluating the mechanical properties with an emphasis on the failure mechanisms of the laser welded DP steel joints under both monotonic and cyclic loading.

2. Materials and experimental procedure

2.1. Materials

The DP600 steel having a thickness of 1.2 mm with a galvannealed (GA) coating (46 g/m^2 at the top and 47 g/m^2 at the bottom) was selected in the study. The chemical composition of the base metal is given in Table 1.

2.2. Laser welding

The laser welding was done using a diode laser and the welding parameters used in the present study are shown in Table 2. The Nuvonyx ISL4000L diode laser head was mounted on a Panasonic VR6 robotic arm. The beam had a rectangular shape with dimensions of 12 mm × 0.9 mm with a focal length of 90 mm. Also, due to the power density of the diode laser it was restricted to conduction mode welding. During welding ultra-high purity argon was used as a shielding gas at a flow rate of 14.2 l/min on both surfaces of the blanks. Welding was conducted at a welding speed of 1 m/min in full penetration bead on a plate mode.[2]

2.3. Microstructure and microhardness testing

The base metal of DP600 steel was cut in three different orientations, i.e., in the longitudinal, transverse, and short transverse directions. Then the specimens were mounted, ground, polished and etched with 2% nital solution for metallographic observations. The cross sectional microstructures of the welded specimens were examined. An optical microscope coupled with Clemex image analysis system was used to observe the microstructural change across the welds. Vickers microhardness tests were performed on the unetched samples. A load of 500 gm and a dwell time of 15 s were used during testing. All the values presented were an average of three series of values taken on the same specimen. The center point of the fusion zone was determined by carefully observing the weld geometry under microscope and all the indentations were ade-

---

[2] Bead-on-plate means a butt weld with full penetration on the blanks of uniform thickness.

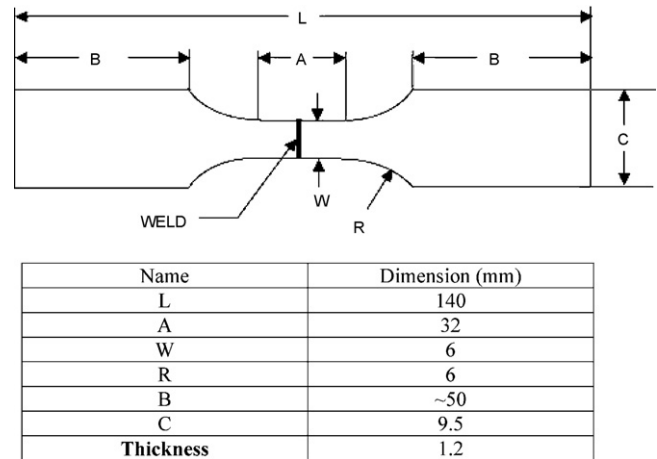| Name	Dimension (mm)
L	140
A	32
W	6
R	6
B	~50
C	9.5
Thickness	1.2

Fig. 1. Geometry and dimensions of the tensile and fatigue test specimens used in the present study.

quately spaced to avoid any potential effect of strain fields caused by adjacent indentations.

2.4. Tensile tests

ASTM-E8 M sub-sized specimens were used for the tensile tests. The geometry of the tensile test sample is given in Fig. 1. The welded samples were machined perpendicular to the welding direction. The gauge area of all the test samples was carefully ground along the loading direction with sand papers up to a grit number of 600. Tensile tests were performed at room temperature using a fully computerized universal tensile testing machine. The strain rates used in the present tensile tests were 0.01 s^{-1}, 0.001 s^{-1}, 0.0001 s^{-1}, and 0.00001 s^{-1}. An extensometer with a gauge length of 25 mm was used to measure the strain during the test. At least two samples were tested at each strain rate. The 0.2% offset yield strength, ultimate tensile strength, and ductility (percent elongation) were evaluated.

2.5. Fatigue tests and fractography

The fatigue tests were conducted using a fully computerized Instron 8801 servo-hydraulic testing system under load control and at more than 6 stress amplitudes. At each stress level two or more samples were tested with the same geometry and dimension as those of the tensile test samples. The stress ratio of R ($\sigma_{min}/\sigma_{max}$) equal to 0.1, sinusoidal waveform, and a frequency of 50 Hz were selected in all the tests. After the fatigue tests the base metal and the welded joints were examined via a JSM-6380LV scanning electron microscope equipped with Oxford energy dispersive X-ray spectroscopy (EDS) system and 3D fractographic analysis, to identify fatigue crack initiation sites and propagation mechanisms.

3. Results and discussion

3.1. Microhardness profile and microstructural change

Fig. 2 shows the micro-indentation hardness profile of laser welded DP600 steel joints. Significantly higher hardness values, approximately 1.5 times higher than that in the base metal, were observed in the fusion zone (FZ). SEM examination of this region indicated that the phases apparent in the FZ included predominantly martensite (M) in conjunction with some sideplate ferrite and bainite (Fig. 3(a)). The formation of martensite in the FZ resulted from the rapid cooling of the weld pool during laser weld-

Table 2
Welding parameters selected in the present study.

Laser machine	Laser source	Laser power (kW)	Welding speed (m/min)	Focal length (cm)	Beam dimension (mm^2)
Nuvonyx ISL-4000	Diode	4	1	9	12×0.9

ing process. In the HAZ the hardness value varied, where the region near the fusion zone had a higher hardness than the region close to the base metal due to the formation of martensite. Similar results were presented in [21]. The region near the base metal in the outer HAZ was observed to have a lower hardness value than the base metal, called the soft zone as indicated in Fig. 2. The presence of the soft zone was mainly due to tempering of pre-existing marten-sitic phase [3,18,19] which could be seen in Fig. 3(b), representing tempered martensite (TM) and bainite in the ferrite matrix, plus some pre-existing retained austenite. Similar results have also been reported in other grades of welded DP steels [17,18,20]. This soft zone would have a detrimental effect on the mechanical proper-ties of laser welded DP600 steel joints, which will be seen in the later sections. The hardness values in the base metal were observed to be nearly constant throughout the material, corresponding to the microstructure of the base metal containing martensite in the ferrite matrix plus some retained austenite (Fig. 3(c)).

3.2. Tensile properties

Fig. 4 shows the engineering stress–strain curves obtained from both the base metal and the welded joints. It is of interest to note that the stress–strain curves of DP600 base metal were smooth and continuous at all the strain rates (Fig. 4(a)), while the welded DP600 joints showed yield point phenomena at all the strain rates as shown in Fig. 4(b). All the welded samples failed at the outer HAZ and an example is shown in Fig. 5, where the vertical lines were the welding marks. Careful observations during the tensile tests showed that the onset of yielding occurred in the softened zone and then the majority of the plastic deformation was accumulated in that zone (i.e., in the outer HAZ) until final failure. The welded joints had higher yield strength than the base metal but the ten-sile strength of the welded specimens was slightly lower than that of the base metal (Fig. 6). While both yield strength and ultimate tensile strength slightly increased with increasing strain rate, the ductility did not show any precise trend with respect to the strain rate (Fig. 7). While ductile type of fracture mode was observed in
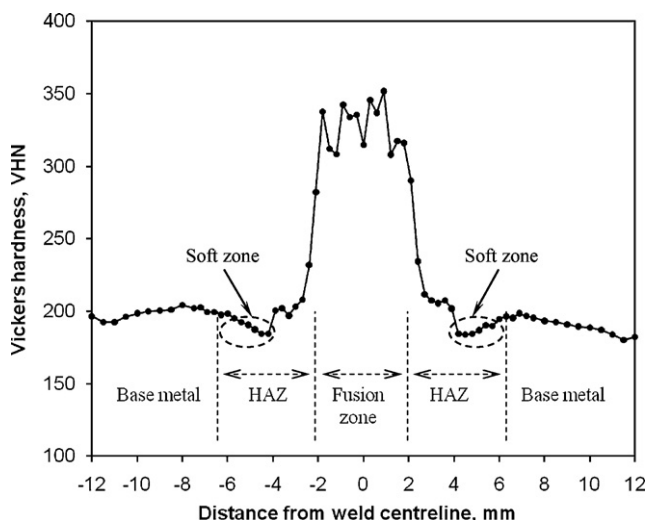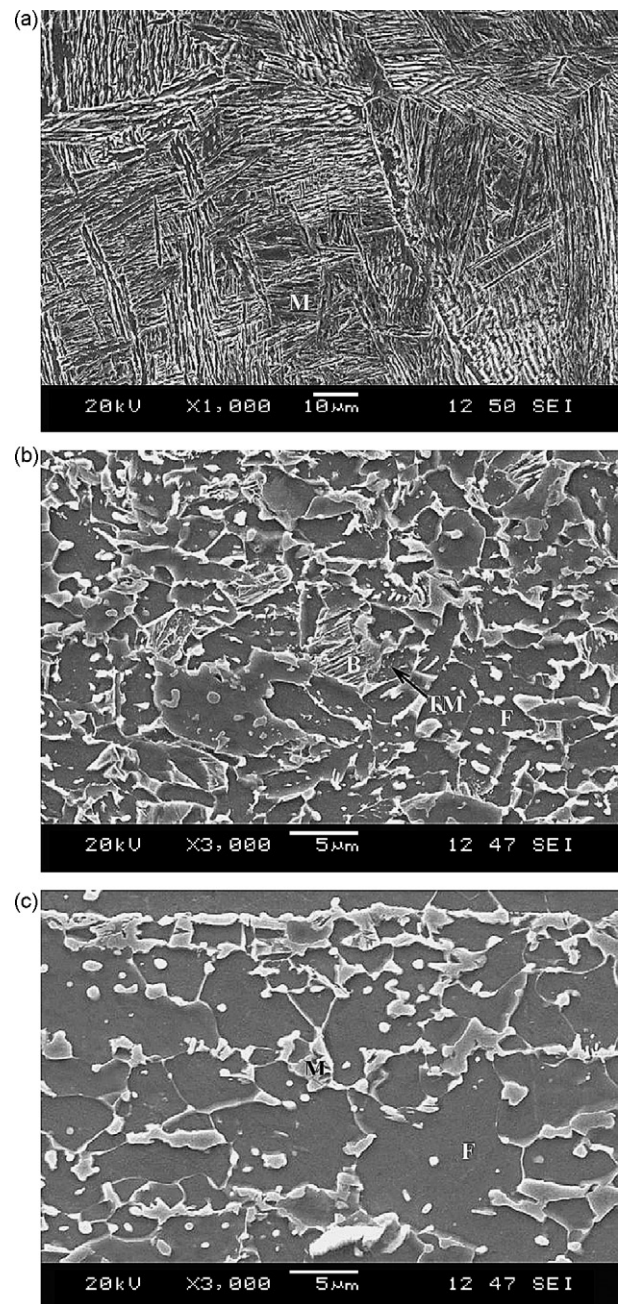

Fig. 3. SEM micrographs showing the microstructural change of a laser welded DP600 steel joints, (a) fusion zone, (b) outer HAZ (soft zone), and (c) base metal, where M, F, B, and TM stand for martensite, ferrite, bainite, and tempered martensite, respectively.

all the tensile test samples, the welding led to a reduction in the elongation (Fig. 7).

The presence of yield point phenomena in the welded samples was likely due to interstitial diffusion which might occur during the laser welding process. The high temperature generated from laser drove the carbon (or nitrogen) atoms in iron to diffuse to the position of the high energy just below the extra plane of atoms in a positive edge dislocation. The elastic interaction was so strong
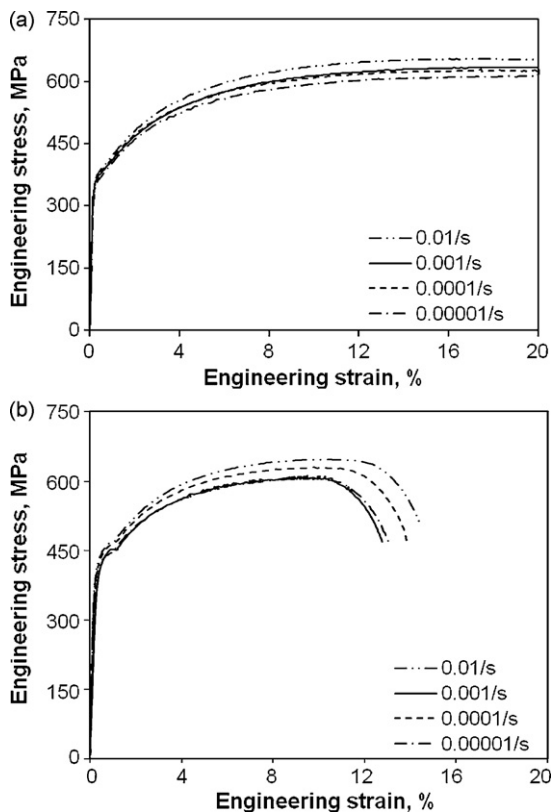

Fig. 2. Typical microhardness profile of the laser welded DP600 steel joint.

Fig. 6. Effect of laser welding on the yield strength and ultimate tensile strength of the DP600 steel tested at different strain rates.

indicating the typical fracture caused by simple tensile loads. The fracture surface near the edge (Fig. 8(b)) showed a combination of both equiaxed and shear dimples as it had a network of dimpled impressions of equiaxed appearance along with dimples having an elongated parabolic shape. This means that shearing motion in this region took place along with the tensile load.

3.3. Fatigue behavior

Load controlled fatigue tests indicated that while the welded joints had a slightly lower fatigue limit than the base metal, almost the same fatigue life between the base metal and welded joints was observed at higher stress amplitudes, as shown in Fig. 9. This result suggested that the slight drop in the hardness in the outer HAZ (Fig. 2) was not large enough to reduce the fatigue strength at higher stress amplitudes. That is, the high stress amplitude overrode the potential negative effect of the soft zone. The obtained fatigue limit and the calculated fatigue ratio of these two groups of material are listed in Table 3. The fatigue limit of the welded joints was about 12.5% lower than that of the base metal, and a fatigue ratio of 0.28 was obtained for the welded joints, in comparison with 0.32 for the base metal. The slight reduction in the fatigue limit or fatigue ratio of the welded samples implied that the negative effect of the

Fig. 4. Engineering stress–strain curves of the DP600 steel tested at different strain rates, (a) base metal and (b) welded joints.

that the impurity atmosphere became completely saturated and condensed into a row of atoms along the core of the dislocation. When such a sample with disloactions pinned by interstitials (i.e., the welded sample in this study) was loaded, a higher stress was required to start the dislocation movement representing the onset of plastic deformation. As a result, the yield strength after laser welding became higher, as shown in Fig. 6. Once the dislocation line was pulled free from the influence of the solute atoms, slip could occur at a lower stress, exhibiting yield point phenomena as seen in Fig. 4(b). Some detailed descriptions on the source of upper yield point which was the drop of the load after the onset of yielding could be seen in the literature [22–24].

Both the welded joints and the base metal showed basically similar features on the fracture surfaces. Cup-like dimple rupture was the main feature of the fracture surface, representing ductile type of fracture mode. Typical SEM micrographs of the fracture surface of the welded sample can be seen from Fig. 8. The fracture surface at the center (Fig. 8(a)) contained mostly equiaxed dimples
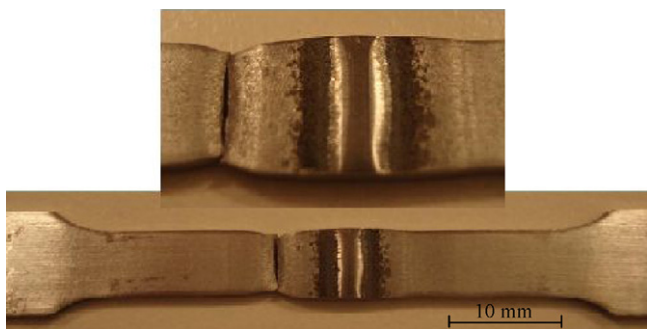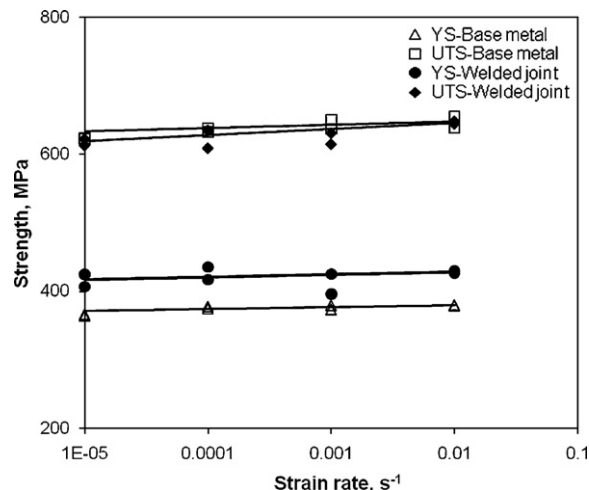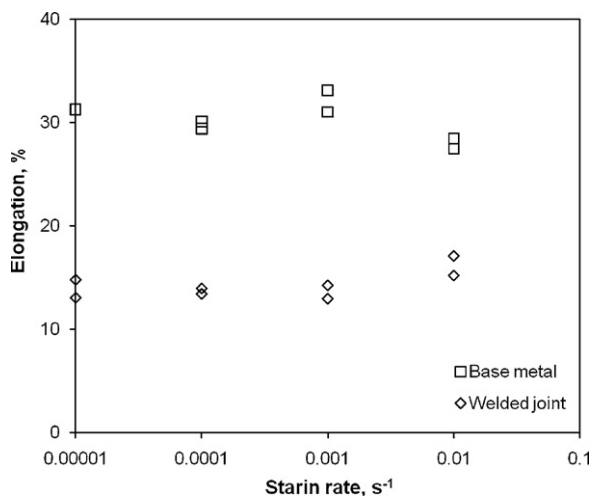

Fig. 5. Typical failure location of the tensile test samples of the laser welded DP600 steel joints.

Fig. 7. Effect of laser welding on the ductility of DP600 steel tested at different strain rates.
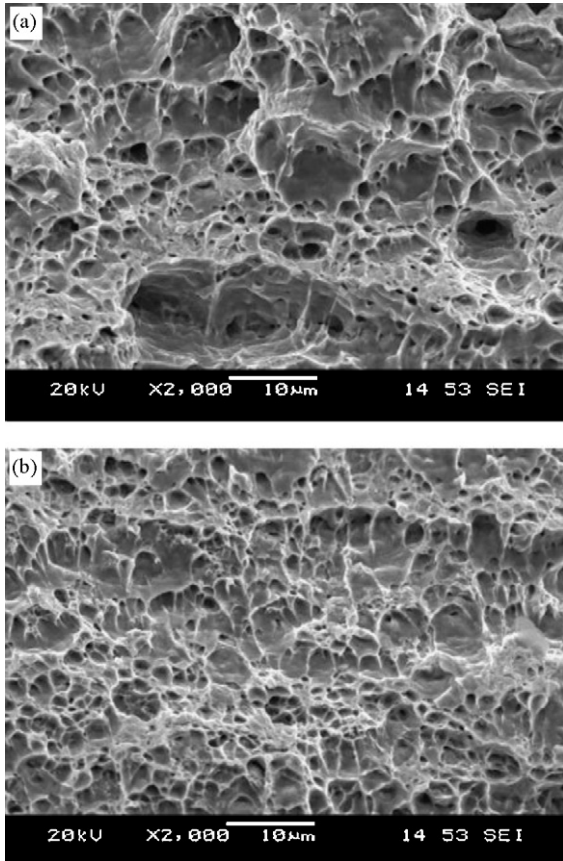
Fig. 8. Typical SEM micrographs of the tensile fracture surface of a welded joint tested at a strain rate of $1 \times 10^{-3}\,\text{s}^{-1}$ (a) in the center and (b) near the specimen surface.
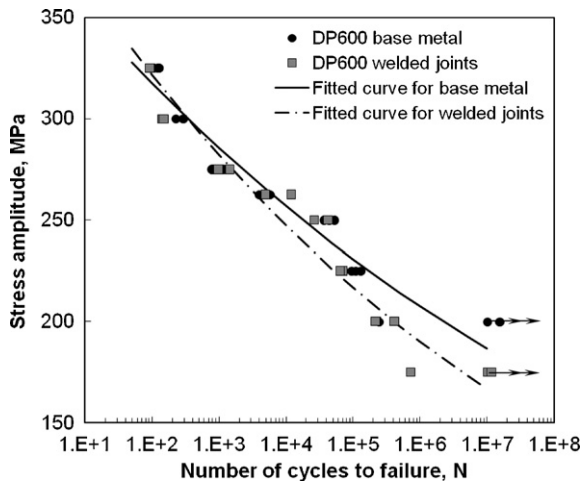

Fig. 9. S–N curves for the DP600 base metal and welded joints tested at $R = 0.1$, 50 Hz, and room temperature, where the data points with arrowmarks indicate the run-out samples.

Table 3
Fatigue limit and fatigue ratio of the DP600 base metal and welded joints.

Material type	Fatigue limit (MPa)	Ultimate tensile strength (MPa)	Fatigue ratio
DP600 base metal	200	634	0.32
DP600 welded joints	175	630	0.28

Table 4
Fatigue parameters σ_f' and b for the DP600 base metal and welded joints.

Material type	σ_f' (MPa)	b
DP600 base metal	405	−0.046
DP600 welded joints	435	−0.057

soft zone in the outer HAZ appeared, which could not be ignored at lower stress amplitudes in the near fatigue limit region.

The following Basquin-type equation was used to fit the fatigue data,

$$\sigma_a = \sigma_f'(2N)^b, \tag{1}$$

where σ_a is the alternating stress amplitude, σ_f' is the fatigue strength coefficient defined by the stress intercept at $2N = 1$, N is the number of cycles to failure and $2N$ is the number of load reversals to failure, and b is the fatigue strength exponent. The values of σ_f' and b for the base metal and the welded sample are given in Table 4. It is seen that the fatigue strength coefficient was higher for the welded joints, but the absolute value of fatigue strength exponent was slightly larger which would give rise to a slightly shorter fatigue life (since a smaller value of b corresponded to a longer fatigue life [24]). As a result, it was similarly difficult to use the σ_f' and b values to distinguish the difference between the fatigue lives of the welded joints and base metal, as demonstrated in Fig. 9.

3.4. Fatigue failure location and mechanism

Regarding the fatigue failure location it was observed that at a stress amplitude of higher than 250 MPa all the welded samples failed at the outer HAZ, and the base metal samples failed within the gauge section. However, at or below a stress amplitude of 250 MPa all the welded samples and base metal samples failed far away from the middle of gauge section. These results corresponded well to the presence of an inflection point on the S–N curves occurred at a stress amplitude of about 250 MPa in both the welded joints and base metal, as shown in Fig. 9. The failure location of the welded sam-
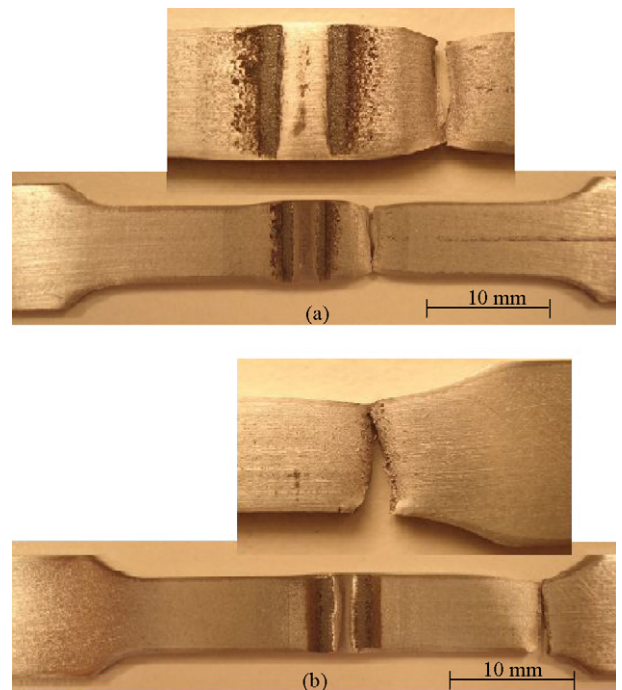

Fig. 10. Typical fatigue failure location of the welded samples tested at a stress amplitude of (a) above 250 MPa, and (b) below 250 MPa.

ples tested at two different ranges of stress amplitudes can be seen in Fig. 10. The possible reason for this effect would be related to cyclic strengthening mechanisms involving deformation-induced martensite transformation [25,26,27]. The DP steel contained a small amount of retained austenite in its microstructure; during cyclic loading the retained austenite transformed to martensite and gave additional strengthening effect in the steel. These martensitic particles were considered to further pin the dislocations and dominate the cyclic deformation [28]. In the LCF region where the samples were tested at a higher stress amplitude the dislocations could overcome the martensite barriers as the applied stress magnitude surpassed the pinning force created by martensite, resulting in more cumulative damage in the gauge section of the test samples. This phenomenon would be the reason why at the higher level of stress amplitudes the failure occurred in the gauge section for both base metal and welded joints. More specifically for the welded samples fatigue failure occurred at the outer HAZ due to the lower hardness (Fig. 2). But in the HCF region where the sample lasted for a longer period of time at a lower level of stress amplitudes, the applied stress could not overcome the pinning force created by the martensite interacting with the dislocations. The area near the end of the gauge section became the weakest area due to potential stress concentration caused by the notch effect. Generally, the

notch effect was reported to be stronger in the longer life HCF region compared to the shorter life LCF region [29].

The fractographic examination of the fatigue fracture surfaces indicated that crack initiation occurred from the surface of the specimens. In both the base metal and the welded joints, the samples tested at or below a stress amplitude of 250 MPa showed clear crack initiation site and crack propagation area on the fracture surfaces. A typical example showing the overall view of the fracture surface of the welded sample tested at a stress amplitude of 225 MPa is shown in Fig. 11(a). Crack initiation took place from the specimen surface (Fig. 11(b)). Surface grains were usually less constrained than the interior grains, so that the occurrence of slip in a few grains near the specimen surface could be relatively easier during fatigue [30]. The back and forth fine slip movements during fatigue could build up notches or ridges at the surface, also referred to as intrusions and extrusions [24]. This kind of notch with a notch root of atomic dimension acted as a stress raiser and might be the nucleation site of the fatigue crack [24]. Surface roughness and protrusions could also act as a site of stress concentration that caused the crack initiation during fatigue. Stage I fatigue crack propagation could be seen near the surface (Fig. 11(b)). Fatigue crack growth indicating stage II crack propagation was mainly characterized by fatigue striations (Fig. 11(c) and (d)), which were usually perpen-
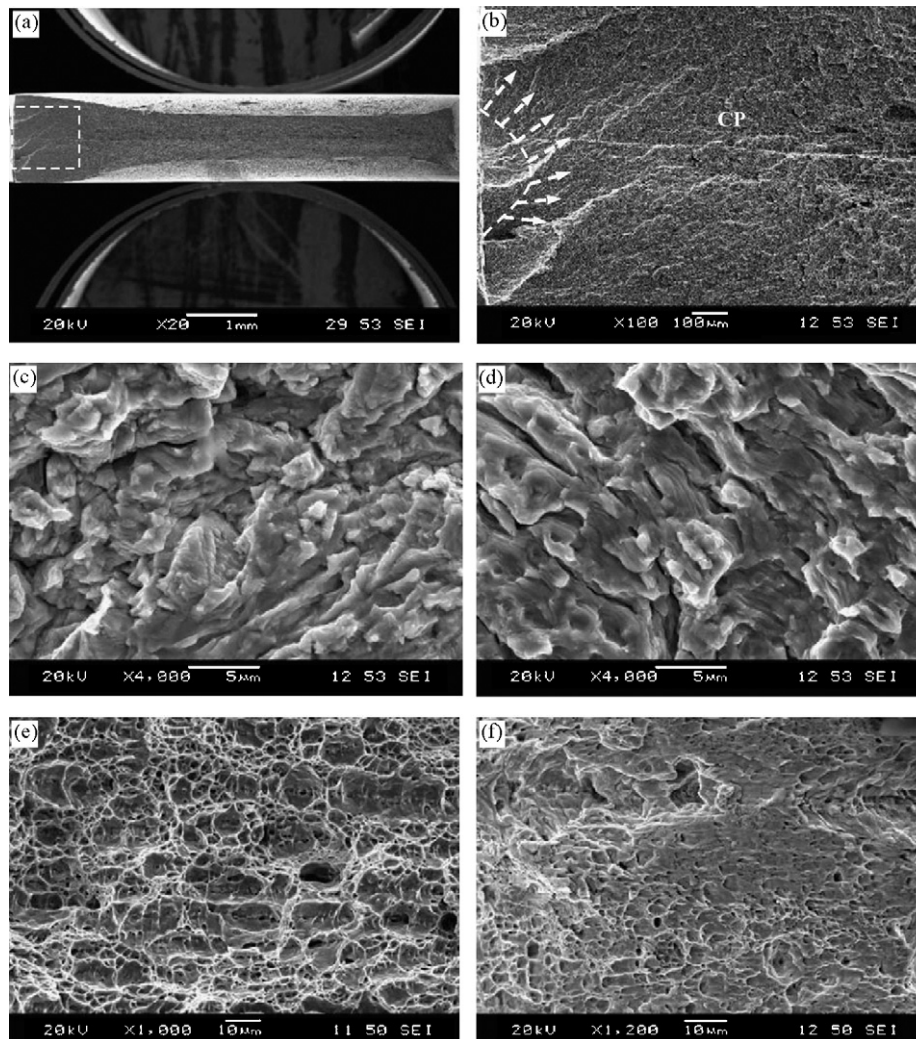

Fig. 11. Typical SEM micrographs of fatigue fracture surface of welded joints tested at a stress amplitude of 225 MPa, (a) overall view of the fracture surface at a low magnification, (b) magnified view of the dashed box in (a) showing crack initiation site and crack propagation area at an intermediate magnification, where CP indicates crack propagation region and the arrows indicate the direction of the crack propagation, (c) crack propagation area close to the crack initiation site at a higher magnification, (d) crack propagation area at about 2 mm from the crack initiation site at a higher magnification with secondary cracks, (e) center of the fracture surface, and (f) near-edge area on the fracture surface.
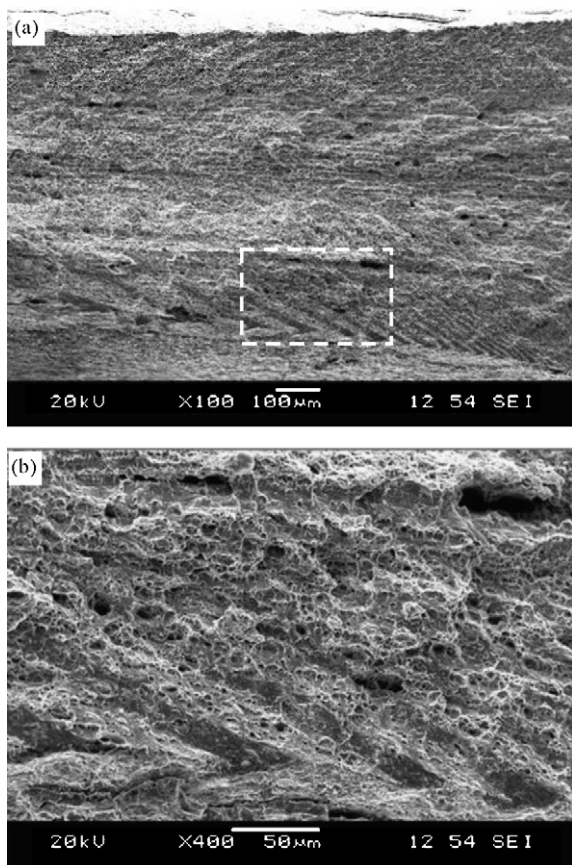
Fig. 12. Fatigue fracture surface of a welded sample tested at a stress amplitude of 250 MPa (a) deformation bands near both specimen surfaces, and (b) a magnified view of the boxed area in (a).

dicular to the propagating direction. The spacing of the striation marks was smaller near the crack initiation site reflecting a slower rate of crack propagation (Fig. 11(c)), whereas at the later stage of crack propagation the increased striation spacing (Fig. 11(d)) represented a faster propagation at the crack front. The formation of fatigue striations was basically considered to be due to a repeated plastic blunting–sharpening process caused by either dislocation slip [31] or twinning [32,33] in the plastic zone at the fatigue crack tip. The secondary cracks were observed in stage II crack propagation as well, as seen in Fig. 11(d). The faster crack propagation at the center of the fracture surface was mainly characterized by the cup-like dimpled rupture being typical of the ductile fracture mode (Fig. 11(e)). The elongated oval-shaped dimples due to the shear motion were the predominant feature near the edge of the fracture surface, representing the final rapid failure of the sample (Fig. 11(f)). Both the base metal and the welded samples had basically similar fracture surface characteristics. However, the samples tested at or below a stress amplitude of 250 MPa showed some deformation bands situated away from the crack initiation site shown in Fig. 12(a) and (b). The formation of the deformation bands was mainly due to the inhomogeneous deformation, caused by the presence of crystallographic texture in the rolled plate [34,35]. Further studies on the effect of texture on fatigue fracture mechanisms in the welded DP600 steel joints are needed.

4. Conclusions

1. The large amount of martensitic structure formed in the FZ due to the rapid cooling during welding led to a considerable increase in the hardness. However, a soft zone in the outer HAZ was observed due to the tempering of the pre-existing martensite in the DP600 steel.
2. While the presence of the outer HAZ softening reduced the ductility to a certain extent, the ultimate tensile strength remained nearly unchanged after laser welding. On the other hand, the welded DP600 steel joints were observed to have a higher yield strength and exhibit slightly yield point phenomena, compared to the base metal.
3. The strain rate dependence of the tensile properties was observed to be weak, since the yield strength and ultimate tensile strength increased only slightly with increasing strain rate from $1 \times 10^{-5}\,s^{-1}$ to $1 \times 10^{-2}\,s^{-1}$ in both base metal and welded joints.
4. Although the fatigue limit and fatigue ratio of the welded joints was slightly lower than that of the base metal, the fatigue life at the higher level of stress amplitudes was almost the same within the experimental scatter between the base metal and welded joints despite the presence of the soft zone.
5. In all cases of the welded samples tested at different strain rates the tensile fracture occurred at the soft zone, but the tensile fracture surfaces still exhibited characteristic dimple/ductile fracture. In both the base metal and welded joints fatigue crack initiation was observed to occur at the specimen surface, and fracture surfaces were characterized by the characteristic fatigue striations. Dimples and some deformation bands were also observed in the fast propagation area.

Acknowledgements

References

[1] Advance High Strength Steel (AHSS) Application Guidelines, International Iron and Steel Institute, 2006, www.worldautosteel.com.
[2] W. Bleck, JOM 48 (1996) 26–30.
[3] M. Xia, E. Biro, Z. Tian, Y.N. Zhou, ISIJ Inter. 48 (2008) 809–814.
[4] S.R. Mediratta, V. Ramaswamy, V. Singh, P. Rama Rao, Trans. Ind. Inst. Metals 38 (1985) 350–372.
[5] D.L. Chen, Z.G. Wang, X.X. Jiang, S.H. Ai, C.H. Shih, Mater. Sci. Eng. A 108 (1989) 141–151.
[6] Z.G. Wang, D.L. Chen, X.X. Jiang, S.H. Ai, C.H. Shih, Scripta Metall. 22 (1988) 827–832.
[7] M. Sarwar, R. Priestner, J. Mater. Sci. 31 (1996) 2091–2095.
[8] H.B. Carry, S.C. Helzer, Modern Welding Technology, 5th edition, Pearson Education Inc., New Jersey, U.S.A., 2005.
[9] C. Ma, D.L. Chen, S.D. Bhole, G. Boudreau, A. Lee, E. Biro, Mater. Sci. Eng. A 485 (2008) 334–346.
[10] F. Rossillon, A. Galtier, J.L. Robert, M. Duchet, A. Lens, H. Oikawa, Weld. World 52 (2008) 30–41.
[11] P.K. Ghosh, P.C. Gupta, R. Avtar, B.K. Jha, ISIJ Inter. 30 (1990) 233–240.
[12] S. Daneshpour, S. Riekehr, M. Koçak, C.H.J. Gerritsen, Sci. Tech. Weld. Join. 14 (2009) 20–25.
[13] R. Koganti, S. Angotti, A. Joaquin, C. Jiang, C. Karas, Proceedings of ASME International Mechanical Engineering Congress and Exposition, IMECE 2007, November 11–15, 2007, Ser. 3, American Society of Mechanical Engineers, Seattle, WA, United states, 2008.
[14] M.P. Miles, J. Pew, T.W. Nelson, M. Li, Proceedings of 2006 TMS Annual Meeting February 13–17, Minerals, Metals and Materials Society, San Francisco, CA, United States, 2005.
[15] J.K. Larsson, Weld. Res. Abroad 49 (2003) 29–45.
[16] K. Chung-Yun, H. Tae-Kyo, L. Bong-Keun, K. Jeong-Kil, Mater. Sci. Forum 539–543 (2007) 3967–3972.

[17] N. Sreenivasan, M. Kuntz, Y. Zhou, Proceedings of Materials Science and Technology Conference and Exhibition, MS and T'07—"Exploring Structure, Processing, and Applications Across Multiple Materials Systems", September 16–20 Ser. 5, Curran Associates Inc., Detroit, MI, United states, 2007.

[18] M. Xia, N. Sreenivasan, S. Lawson, Y. Zhou, Z. Tian, J. Eng. Mater. Technol. Trans. ASME 129 (2007) 446–452.

[19] M.S. Xia, M.L. Kuntz, Z.L. Tian, Y. Zhou, Sci. Tech. Weld. Join. 13 (2008) 378–387.

[20] N. Sreenivasan, M. Xia, S. Lawson, Y. Zhou, J. Eng. Mater. Technol. Trans. ASME 130 (2008) 0410041–0410049.

[21] S. Kou, Welding Metallurgy, 2nd edition, John Wiley & Sons Inc., USA, 2003.

[22] H.K.D.H. Bhadeshia, R.W.K. Honeycombe, Steels—Microstructures and Properties, 3rd edition, Butterworth-Heinmann, Oxford, UK, 2006.

[23] W.D. Callister Jr., Material Science and Engineering—An Introduction, 7th edition, John Wiley & Sons Inc., New York, USA, 2007.

[24] G.E. Dieter, Mechanical Metallurgy, SI Metric edition, McGraw-Hill Book Co., UK, 1988.

[25] T.B. Hilditch, I.B. Timokhina, L.T. Robertson, E.V. Pereloma, P.D. Hodgson, Metall. Mater. Trans. 40A (2009) 342–353.

[26] X. Cheng, R. Petrov, L. Zhao, M. Janssen, Eng. Fract. Mech. 75 (2008) 739–749.

[27] K. Sugimoto, M. Kobayashi, S. Yasuki, Metall. Mater. Trans. 28A (1996) 2637–2644.

[28] P. Lukas, L. Kunz, Fatigue Fract. Eng. Mater. Struct. 25 (2002) 747–753.

[29] M. Sauzay, P. Gilormini, Fatigue Fract. Eng. Mater. Struct. 23 (2000) 573–579.

[30] K.S. Chan, P. Yi-Ming, D. Davidson, R.C. McClung, Mater. Sci. Eng. A 222 (1997) 1–8.

[31] C. Laird, ASTM Spec. Tech. Publ. 415 (1967) 131–168.

[32] S. Begum, D.L. Chen, S. Xu, A.A. Luo, Metall. Mater. Trans. A 39A (2008) 3014–3026.

[33] S. Begum, D.L. Chen, S. Xu, A.A. Luo, Mater. Sci. Eng. A A517 (2009) 334–343.

[34] B.J. Duggan, C.S. Lee, R.E. Smallman, Mater. Sci. Forum 157–6 (1994) 1759–1764.

[35] B.J. Duggan, Y.Y. Tse, H. Ning, M.Z. Quadir, Proceedings of the 13th International Conference on Textures of Materials, August 26–30 Ser. 408–412, Trans Tech Publications Ltd., Seoul, Korea, 2002.